A Generalized Scaling Theory for Spontaneous Spreading of Newtonian Fluids on Solid Substrates

Amir Azimi Yancheshme[a], Giuseppe R. Palmese[a], Nicolas J. Alvarez[a]

[a]*Chemical and Biological Engineering, Drexel University, Philadelphia, PA 19104, USA*

Abstract

Hypothesis: There exists a generalized solution for the spontaneous spreading dynamics of droplets taking into account the influence of interfacial tension and gravity.
Experiments: This work presents a generalized scaling theory for the problem of spontaneous dynamic spreading of Newtonian fluids on a flat substrate using experimental analysis and numerical simulations. More specifically, we first validate and modify a dynamic contact angle model to accurately describe the dependency of contact angle on the contact line velocity, which is generalized by the capillary number. The dynamic contact model is implemented into a two-phase moving mesh computational fluid dynamics (CFD) model, which is validated using experimental results.
Findings: We show that the spreading process is governed by three important parameters: the Bo number, viscous timescale $\tau_{viscous}$, and static advancing contact angle, θ_s. More specifically, there exists a master spreading curve for a specific Bo and θ_s by scaling the spreading time with the $\tau_{viscous}$. Moreover, we developed a correlation for prediction of the equilibrium shape of the droplets as a function of both Bo and θ_s. The results of this study can be used in a wide range of applications to predict both dynamic and equilibrium shape of droplets, such as in droplet-based additive manufacturing.

Keywords: Droplet spreading dynamics, dynamic contact angle, equilibrium droplet shape, CFD

1. Introduction

The spreading of a liquid droplet on a solid substrate is an important process for a range of industrial applications such as ink-jet printing technologies, fabrication of optical lenses, and additive manufacturing [1, 2, 3, 4]. One of the main challenges in these applications remains the precise control of droplet spreading dynamics and the final droplet shape [5].

Spreading of a Newtonian droplet on a substrate is a complicated phenomena that can depend on several forces, whose magnitudes depend on different time and length scales. For example, let's consider the spreading of a droplet whereby inertial impact of the droplet is ignored. The radius of the three phase contact line is referred to as the basal radius, $R(t)$, and moves outward from initial contact point $R(t = 0) = 0$. When a drop contacts a surface, the amount of spreading is determined by the free energy, which is a function of the surface/interfacial tensions and gravity. The rate of spreading is determined by both fluid inertia and viscous dissipation [6].

Spreading stops when equilibrium is established at the contact line, i.e., when the droplet contact angle balances the Young-Lapalce equation. In the absence of gravity, the Young-Laplace equation reduces to the Young equation [7]:

$$cos\theta_s = \frac{\sigma_{SG} - \sigma_{SL}}{\sigma_{LG}} \tag{1}$$

where θ_s is the static advancing contact angle, and σ_{SG}, σ_{SL}, and σ_{LG} are the surface tension between solid and gas phase, the surface tension between solid and liquid, and the interfacial tension between liquid and gas, respectively. For the special case of complete wetting (i.e. $\theta_s = 0$), a precursor film is formed and the droplet spreads such that a film covers the entire substrate [8].

The influence of gravity on $R(t)$ is determined by the ratio of forces (i.e. gravitational and capillary forces), which is known as the Bond number ($\mathrm{Bo} = \frac{\rho g R_0^2}{\sigma}$). For droplets with low Bo number, i.e. $\mathrm{Bo} << 1$, the effect of gravity on the spreading process can be neglected and capillary force drives the spreading, a.k.a the capillary spreading regime. In this regime, the droplet takes the shape of a spherical-cap during the spreading process [9]. For $\mathrm{Bo} >> 1$, the gravitational force drives the spreading and flattens out the free surface of the droplet, which is referred to as the gravitational spreading regime [9]. The rate of spreading is determined by the ratio of resistive forces (i.e. viscous and inertia forces). A dimensionless group that quantifies the relative magnitude of inertial forces and viscous forces is the Ohnesorge number, i.e. ($\mathrm{Oh} = \frac{\mu}{\sqrt{\rho \sigma R_0}}$). The Oh number can be understood as the ratio of the viscous velocity to the inertial velocity [6]. One might expect that the rate of spreading of droplets with large Oh number are controlled by the droplet viscosity, whereby spreading at low Oh is controlled by inertia. In other words, one might expect different spreading behaviors for different Oh. However, the effect of Oh on spreading dynamics has not been systematically investigated.

There are two main spreading regimes before steady state, namely an initial fast, inertia-controlled stage [10, 6, 11] followed by a final slow, viscous-controlled stage [12, 13, 14, 8]. Several reports in the literature show that the initial spreading stage has a power-law dependence on time, namely $R(t) \propto t^{1/2}$ [6, 11, 15, 10]. However, Bird et. al. reported that for non-zero θ_s, the power law is lower than one half, and depends on the magnitude of θ_s [16]. de Ruijter et al. [17] derived an asymptotic solution for the early-time dynamics at high values of θ_s, and showed that $R(t) \propto t$. Furthermore, the power-law has been argued to also depend on the magnitude of the viscosity, such that at higher viscosity the spreading does not follow a simple power-law [10]. The duration of inertia-controlled spreading is proportional to the propagation of a capillary wave through the droplet interface [18, 19, 16], which is on the order of milliseconds for droplets whose diameter is smaller than the capillary length scale, $l = \frac{\sigma}{\rho g}$ (or alternatively when $\mathrm{Bo} << 1$) [6]. The transition between the initial and final spreading (a.k.a crossover timescale) is argued to be independent of the surface morphology and chemistry of the solid substrate [20, 16]. Thus, the transition between spreading regimes is predominately controlled by the diameter of the droplet. However, it has been reported that the crossover timescale does depend weakly on the fluids properties [6].

Unlike the initial stage, the final spreading stage is argued to depend on the fluid properties, effect of gravity, and the solid substrate properties, i.e. the thermodynamic wetting equilibrium

(θ_s [21, 22, 8, 13]. Historically, the viscous spreading stage follows a power-law scaling with time. For pure capillary driven spreading (i.e. Bo << 1), the final spreading stage for a viscous drop with complete wetting of the substrate is expected to follow Tanner's law, i.e. $R(t) \sim t^{0.1}$ [23], while for gravitational spreading, i.e. Bo >> 1, $R(t) \sim t^{1/8}$ [24, 25]. For intermediate Bo, there is a transition from capillary spreading to gravitational spreading when the basal radius reaches the capillary length. In this regime, Cazabat and Stuart [14] experimentally showed that the late stage of spreading can be described by a sequence of power laws. Although Tanner's and other power-law models have significant historical relevance, the models only offer scaling laws and do not accurately depict the basal radius or height of the droplet as a function of time. Furthermore, data reported over the past two decades show that not all fluid and surface pairs follow Tanner's law even though their Bo is small, such as in the case of partial wetting conditions [26, 27, 28, 29, 30].

The spreading dynamics have been shown in the literature to be significantly slowed for non-zero static advancing contact angles, a.k.a partial wetting conditions, which is typical of most fluid-solid systems [10, 11, 16]. de Ruijter et al. [17] reported $R(t) \sim t^{0.1}$ followed by an exponential relaxation, $R(t) = R_{eq} exp(t/\tau)$, until the equilibrium is achieved, where R_{eq} and τ are final basal radius and a characteristic time scale, respectively. Such exponential relaxation behaviour after Tanner's power-law regime has also been reported by [29, 31]. It has been shown that the duration of each regime, i.e. Tanner's power-law and consequent exponential relaxation, is quite sensitive to the θ_s. The transition from power-law to exponential relaxation is argued to occur when the dynamic contact angle reaches nearly two times θ_s [29]. Wang et al. [32] proposed an empirical exponential-power law correlation to cover the evolution of basal radius for partially wetting fluids as $R(t) = R_{eq}[1 - exp(-\frac{a}{R_{eq}} t^m)]$, where a and m are fitting parameters. However, using such equations to predict the spreading dynamics is limited as they contain fitting parameters with no physical meaning and require the value of equilibrium basal radius, R_{eq}. Moreover, most of the studies on the spreading of partially wetting systems ignore the effect of gravity and only consider the capillary spreading regime, which precludes their use in practical applications with reasonable Bo. These facts highlight the importance of developing a generalized approach for predicting spreading dynamics for a wide range of Bo numbers. Ideally one would like to develop an analytical model to describe the dynamics of spreading, however, there is still questions regarding the appropriate boundary conditions that satisfy the physics. Furthermore, the lack of appropriate boundary conditions prevents the implementation of numerical techniques.

The physics of Newtonian drop spreading has been thoroughly investigated with theoretical approaches based on a total energy balance [33, 34, 35, 36], classical hydrodynamics [13, 37, 38], and molecular kinetic theory [39, 40]. Analytical modeling of spreading dynamics are quite complex, especially when considering gravitational effects. Thus analytical models in the literature either neglect the effect of gravity or over simplify the solution by assuming a shape of the droplet [41]. For example, Reznik and Yarin [42] studied the spreading of an axisymmetric droplet under the dominant action of gravity at large Bo numbers,i.e. $2 < Bo < 15$, through a semi-analytical approach. Their approach required several simplifications, such as: (i) assuming a 2d-wedge model at the contact line, (ii) neglecting the effect of the contact line's curvature on the flow, (iii) assuming a small Ca number approximation, (iv) and assuming creeping flow inside the droplet, which is not necessarily valid for high Bo numbers or low

viscosity fluids. Overall, analytical solutions are limited in their ability to generalize spreading dynamics of Newtonian fluids either in their limits of relevant parameters, such as Bo and Ca, or in their many assumptions. We argue that numerical simulations offer the most general approach to develop generalized spreading dynamics for all Bo and Ca [41]. However, to develop a comprehensive numerical solution to the spreading problem of a Newtonian fluid, the governing physical boundary conditions need to be fully resolved and validated, especially at the triple contact line [43, 44, 45].

The literature has suggested that the spreading dynamics can be accurately predicted by introducing two boundary conditions: (1) the slip velocity (or shear stress) required at the contact line to relax the stress singularity, and (2) the description of the dynamic contact angle during spreading [46]. The literature overwhelmingly agrees that the slip velocity at the contact line is necessary to remove the stress singularity, and has little to no affect on the far-field flow domain [47]. In other words, the slip velocity does not affect the overall shape of the fluid domain and in some regard can be selected arbitrarily. On the other hand, many studies have proposed models for dynamic contact angle, all of which significantly affect the shape of the droplet (i.e. far-field effect) [46]. Many studies have shown there is a generalized dependence of the dynamic contact angle on the contact line velocity and derived an expression for the dynamic contact angle as a function of capillary number, Ca, defined as $\mathrm{Ca} = \frac{\mu u}{\sigma}$ and θ_s,i.e. $\theta_D = \theta_D(\mathrm{Ca}, \theta_s)$. [48]. The exemplary theoretical models of Hoffman-Voinov-Tanner[49] and Cox[38] are worth mentioning. Empirical correlations developed by Jiang et. al [50], Bracke et al. [51] and more recently Kistler [52] have shown a good agreement with experimental dynamic contact angle data of certain fluids at a given range of Ca number. However, it has been shown that in some cases, especially high Ca numbers, these models fail to capture experimental trends [53]. There is an important need for the generalization of dynamic contact angle dynamics for the development of an accurate numerical spreading model.

Although there are numerous papers on a wide variety of drop spreading phenomena, the literature still lacks a generalized solution for spreading dynamics that takes into account both capillary and gravitational effects for full span of spreading (literature mainly focuses on $\mathrm{Bo} << 1$) [41]. Furthermore, there is a need for a generalized validated numerical model that can accurately predict spreading dynamics for a wide range of fluid parameters, contact angles, and stages of spreading. In this work, we develop a numerical method to solve the free boundary problem of drop spreading on a substrate in the absence of impact. Our model is founded on the principle that the dynamic contact angle is explicitly independent of material parameters, and only depends on the Ca and θ_s. This model is experimentally validated and the results are generalized into master curves that take into account the effects of gravity and partial wetting. Thus, these results determine the validity of the zero Bond number approximation in spreading dynamics. The master curves require that the spreading time be normalized by the viscous timescale, τ_v. Ultimately, the spreading dynamics of Newtonian droplets are shown to only depend on three parameters: Bo number, θ_s, and τ_v. The master curves readily predict the shape of a droplet at a certain dimensionless time for a specific Bo and θ_s. Moreover, we develop a correlation to predict the steady state shape of a Newtonian droplet as a function of Bo number and θ_s.

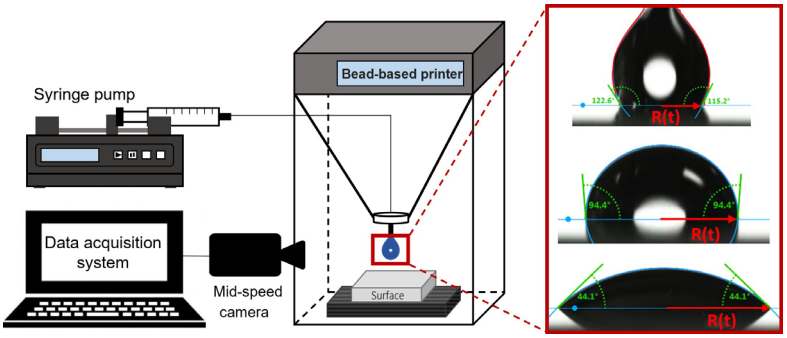

Figure 1: Schematic representation of experimental set up, measured dynamic contact angle and basal radius.

2. Materials and methods

2.1. Experimental data

We developed an *in-situ* device for depositing and monitoring the spreading of gently deposited pendant drops onto a microscope glass slide (AmScope^{TM}). The experimental setup consisted of a digital camera (HAYEAR, HY-2307, 2M pixels with pixel size of $1.43_{\times}1.43$ μm) and a microscope zoom lens. Images were acquired at 60 frames/sec and based on the adjusted magnification of the lens, an example image calibration was 61 pixels/mm, or 16 μm/pixel. Therefore, the minimum distance (i.e. smallest details) detectable between objects is 16 microns. A syringe pump (HARVARD Apparatus, PHD 2000) with minimum flow rate of 0.0001 μL/hr and accuracy of 0.35% connected to a 25 gauge needle (OD=0.51 mm) with an adjustable height was used to carefully dispense and deposit the droplet onto the glass slide from a controlled height (Fig. 1). The microscope slide was washed and rinsed subsequently using Isopropanol (VWR, CAS No. 67-63-0) and DI water (EMD Millipore Corporation) before each test. Three Newtonian fluids i.e. Glycerin (Cococare Products, Inc., CAS No.56-81-5), Light corn syrup (Karo®, CAS No.8029-43-4), and a photo-curable resin called DA2[54] were used as test fluids. Note that the test fluids were chosen to span a range of viscosities between 0.1-10 Pa$\cdot$s, which correspond to a range of Ohnesorge numbers between 0.6 and 15. This range of viscosities allows for the testing of a generalized theory for droplet spreading on both sides of Oh=1. Recall that we hypothesize that spreading physics can be normalized to generate a master curve that is not dependent explicitly on viscosity. Thus any conclusions on experimental validation of a spreading master curve is limited to the experimental viscosity range studied here. However, we do not expect to observe any differences for lower or higher fluid viscosity outside of the experimental window. Each experiment was performed at least three times. ImageJ software (ImageJ.Ink, V. 1.46) and a custom matlab code were used to measure the dynamic contact angle and basal radius as a function of time during spreading (Fig. 1). We also used the reported drop spreading data in the literature (i.e. dynamic contact angle and basal radius vs time) of poly(propylene glycol), PPG [32] and silicone oil [55] along with our measured experimental data to further validates our models and simulations. Table 1 summarizes the properties and equilibrium wetting data of each fluid.

Table 1: Fluid properties and wettability conditions used in experiments and the ones extracted from the literature.

Fluid	ρ **(kg/m^3)**	σ **(mN/m)**	μ **(Pa.s)**	$\mathbf{R_0}$ **(mm)**	θ_s **(deg.)**
Glycerin	1377	63.4	0.74	1.10	20.9 ± 0.3
Corn syrup	1503	42.3	4.18	1.10	46.2 ± 0.8
DA2 resin	1105[54]	35.1	0.49	1.01	19.6 ± 1.4
Silicone oil [55]	970	20.9	0.19	0.34	0
poly(propylene glycol)(PPG) [32]	1010	32.3	0.11	0.98	0

2.2. Numerical modeling and simulation

This work involves a comprehensive numerical approach to simulate drop spreading using COMSOL Multiphysics® v.5.6. Given the drop spreading is a free boundary problem with moving contact line, we employed a laminar isothermal two-phase moving mesh interface (an Arbitrary Lagrangian – Eulerian (ALE) formulation) for all of the simulations. The two phase moving mesh method is known for its high accuracy and lower computational loads in comparison with other multiphase modeling methods such as phase field and level set methods. However, this approach has some intrinsic limitations which cannot handle topographical changes. All of the simulations were solved using a 2D-axisymmetric framework to reduce computation time. Future work could examine the spreading of asymmetrical droplets using a 3D model. Figure S1 shows a schematic of droplet deposited on a substrate and its 2-dimensional view (axisymmetric) profile with an example mesh grid used in our computational model.

2.2.1. Governing equations

The pressure, p, and velocity field ($\bar{u}$) of the computational domain were determined using the Navier-Stokes (N-S) and continuity equations given by,

$$\rho \frac{\partial \bar{v}}{\partial} + \bar{v} \cdot \bar{\nabla} \bar{v} = -\bar{\nabla} p + \mu \nabla^2 \bar{v} + \bar{g} \tag{2}$$

$$\bar{\nabla} \cdot \bar{v} = 0 \tag{3}$$

where ρ is the density, μ is the dynamic viscosity, and $\bar{g}$ is the gravitational acceleration. The problem was solved in 2D-axisymmetric coordinates. Note that there are two N-S equations, one for each fluid phase. The difficulty of the problem lies in solving for the moving liquid-air boundary, S, whose normal velocity, V_S, is directly related to the bulk fluid velocity field assuming continuity of velocity,

$$V_S = \bar{n} \cdot \bar{v}^I = \bar{n} \cdot \bar{v}^{II} \tag{4}$$

Where $\bar{n}$ denotes the unit normal vector, and the superscripts I and II denote the respective fluid phase. The motion of S must satisfy the normal stress balance at the interface given by,

$$\bar{n} \cdot (\bar{T}^I - \bar{T}^{II}) = \sigma(\bar{\nabla} \cdot \bar{n})\bar{n} - \bar{\nabla}\sigma \tag{5}$$

where $\bar{T}$ is the total stress, i.e. $p\bar{I} - \bar{\tau}$, and the RHS represents the force per unit area due to surface tension, σ. A constant atmospheric pressure was applied at the interface. Although we initially included the N-S equations for both phases, we found that the contribution from the air phase was inconsequential. Thus, the surrounding air was assumed to be stagnant at all

times, except at the interface. In other words, the effect of the fluid flow in the air phase during spreading was too small to measure. This assumption was validated by performing several larger scale simulations where the fluid mechanics in the surrounding air was explicitly solved for, see Fig. S2, and comparing these results with the assumption of a stagnant air phase. The results clearly show that for the conditions considered, the air phase kinematics could be ignored.

2.2.2. Initial conditions

The numerical scheme requires an initial shape of the interface at $t = 0$. A logical choice is a pendant drop shape which intersects with the substrate at a single point. However, this proved a poor initial condition as the single contact point was the cause of significant convergence issues[1]. Instead, we used an initial non-zero contact between the bead and substrate at $t = 0$, see Fig. S1. This initial interface condition resembles the start of the spreading process, as a certain amount of contact between the bead and printing bead is inevitable at the onset of spreading. To minimize the effect of this initial condition on spreading dynamics, we simulated the spreading process using different initial contact lengths and shifted the spreading results in time to compensate the initial contact, and showed that for relatively small contact lengths, i.e. 30% of drop diameter, the spreading dynamics were independent of the initial contact length (see Fig. S3) regarding the initial pendant drop shape, we also did two simulations one with an initial pendant drop shape and the other with a spherical shape having the same volume as pendant drop. We showed that the assumption of initial spherical shape instead of pendant drop shape is quite acceptable for droplet spreading process as immediately after detachment of droplet it turns into a spherical shape (Fig. S4). Initially, all phases are assumed to be at rest with $\bar{u} = 0$ and a Laplace pressure across the interface given by ($\Delta p = 2\sigma/R_0$). This condition resembles gentle deposition of a droplet on the printing bed.

2.2.3. Dynamic contact angle and relaxation of stress singularity

At the triple contact line (i.e. intercept of the interface, substrate, and surrounding air), the contact angle of fluid serves as a boundary condition to correctly model the motion of S [56]. It is well-known that the contact line needs to be modeled considering a dynamic contact angle instead of a static advancing contact angle in order to capture correct spreading physics [56, 53]. The typical relationship is the dependence of θ_D on the contact line velocity. Thus, several experiments were performed for Glycerin, Corn syrup and DA2 resin measured in this study, and also propylene glycol (PPG) [32] and silicone oil [55] found in the literature (Table 1) to determine the dependence of contact angle on contact line velocity. The results are shown in Fig. 2a. Several researchers have argued a universal scaling exists for dynamic contact angle. For example, Jiang et al. [50] argued that a universal scaling behavior results when the dimensionless contact angle is plotted versus Capillary number. One empirical model used to describe this universal behaviour was developed by Jiang et al. [50], and is given by:

$$\frac{\cos(\theta_s) - \cos(\theta_D)}{\cos(\theta_s) + 1} = \tanh(A\mathrm{Ca}^B) \tag{6}$$

where A and B are fitting parameters.

Figure 2b shows the experimentally measured values of normalized dynamic contact angle as a function of the Ca number. The Chosen fluids and operational conditions cover a wide range of viscosities from $0.1 Pa.s$ to 5 Pa · s and a wide range of Ca from 10^{-6} to 0.1. It can be concluded

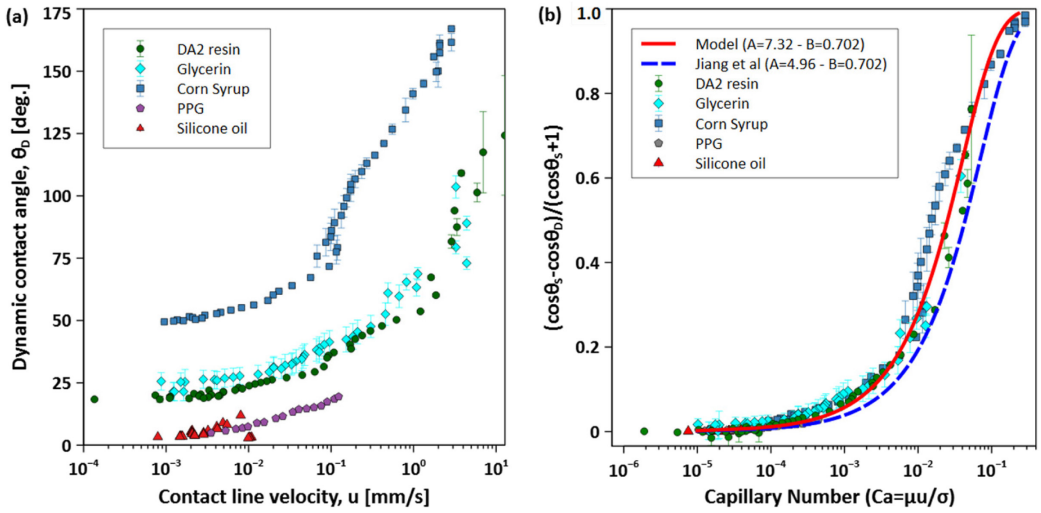

Figure 2: **a)** Dynamic contact angle data versus the contact line velocity for Glycerin, Corn syrup, and DA2 resin measured in this study as well as the extracted experimental data of PPG and silicone oil reported in [32] and [55], respectively, **b)** normalized dynamic contact angle data versus Ca number.

that normalizing the values of dynamic contact angle with the static advancing contact angle ($\frac{cos\Theta_S - cos\Theta_D}{1+cos\Theta_S}$) and plotting them against Ca number generates a master curve for all fluids as a function of Ca. Jiang et al. [50] reported the best fit universal scaling parameters for Eq. 6 as $A = 4.96$ and $B = 0.702$. However, as depicted in Fig. 2b, the parameters reported by Jiang et al. significantly under predicts the values of the dynamic contact angle for a wide range of Ca numbers, especially mid to high Ca. Therefore, we determined the best fit coefficients to be $A = 7.32$, keeping $B = 0.702$, which captures the spreading behavior of all the experimental data presented in Fig. 2 to significantly more accuracy. Thus, Eq. 6 with $A = 7.32$ and $B = 0.702$ is used for all spreading simulations. Note that the ability to fit all experimental data with a single empirical model that does not depend explicitly on fluid parameters is fundamental in developing generalized spreading trends. This model has been previously shown to work for a limited range of fluids, whereas here we show that it works for a wide range of fluid parameters. Furthermore, this empirical model allows for the simulation of droplet spreading of near perfect wetting cases, i.e. Silicone oil and PPG on glass substrate. Typically, the perfect wetting case introduces the added complexity of a precursor film, which one might argue would deviate from the universal dynamic contact angle model. However, for PPG and silicone oil, which are reported to have near zero steady advancing contact angles [55, 32], there appears to be no deviation.

In order to remove the stress singularities at the contact line, as shown in Fig. S1, the liquid-solid interface was modeled using a Navier-slip condition with no-penetration, i.e. ($\bar{u} \cdot \bar{n}_{wall} = 0$), which exerts a shear stress, $\bar{\tau}_f$ on the fluid-substrate contact proportional to the fluid velocity such that,

$$\bar{\tau}_f = \mu \frac{\bar{u}}{\beta}, \tag{7}$$

where β is the slip length and is typically equal to a fraction of the interface mesh element size, $\Delta\bar{x}$ [1, 57]. In this work we considered $\beta = 1/5\Delta\bar{x}$, however, it should be noted that the spreading behaviour is quite insensitive to the values of β. Figure S5 shows that for a range of $\beta = \Delta\bar{x}$ to

$1/10\Delta x^{-}$, the spreading behaviour does not change significantly.

2.2.4. Model validation and spatial convergence

Model spatial convergence was determined by a systematic study of the effect of mesh element size on the time evolution of the basal radius, $R(t)$. We used the parameters for DA2 resin as reported in Table 1 and varying number of mesh points. Note that we intentionally refined the mesh near the triple point contact by scaling the mesh points down by a factor of 0.2. Furthermore, an automatic remeshing constraint was applied to rebuild the entire domain when the quality of mesh falls below 0.1. Figure S6 shows grid independent test results, see Supplementary Information. Below the mesh size of $R_0/40$, refining the mesh points does not improve the solution considerably. Therefore, we used the mesh size criteria of $R_0/40$ for all of the simulations to make sure the results are independent of the mesh size. To validate our numerical model, we compare model results with the experimental spreading behavior of (i) Glycerin, (ii) Corn syrup, (iii) DA2 resin, all on microscope glass slides,(iv) a non-volatile silicone drop on a soda-lime glass substrate, and (v) the spreading of a poly(propylene glycol), PPG solution on microscopic glass slide all reported in Table 1. These five data sets were chosen to cover a wide range of viscosity.

Both PPG solution and silicone oil were simulated considering $\theta_e = 0$ in Eq. 6, i.e. a complete wetting condition at long times [32, 55]. Glycerin, Corn Syrup, and DA2 were simulated using the static advancing contact angles measured in this study and reported in Table 1. Figure 3 shows the model prediction along with corresponding experimental data of basal radius as a function of time for all fluids. The model predictions are in excellent agreement with experimental results with maximum relative error of less than 5% for all fluids. Furthermore, the numerical model shows that at longer times silicone oil and PPG solution both spread with a power-law of $R(t) \sim t^{0.104}$ and $R(t) \sim t^{0.092}$, respectively. Note that both power-laws are very close to the power-law expected from Tanner's law (i.e. $R(t) \sim t^{0.1}$) for a complete wetting system, $\theta_s = 0$.

3. Results and discussion

Spontaneous spreading of a drop after touching the substrate is driven by gravitational, F_g and surface tension, F_c, forces and resisted by viscous, F_μ and inertia, F_i forces. The driving and resistive forces for an initially spherical droplet are summarized in Table 2. It is convenient to discuss the importance of these driving forces on droplet spreading in terms of key dimensionless parameters including Bo, Oh, and Ca numbers.

The Bond number, Bo, which is the ratio of F_g to F_s, represents the relative effect of gravity on the shape of droplet. The effect of gravity on spreading dynamics can be generally ignored provided that the Bo is sufficiently small, i.e. Bo $<<$ 1 [58]. The Ohnesorge number, Oh, commonly used to parameterize inkjet printing [59], but can generally be used to think of the tendency of a droplet/jet to stay together, i.e. not forming satellite droplets, resisting against spreading, etc. Oh number is the ratio of viscous forces to surface stress forces defined as the ratio of F_μ to the square root of F_i and F_c. For Oh $>$ 1, i.e. high viscosity and small radii, the spreading slows down and drops tend to retain a spherical cap-like shape during spreading. Finally, the capillary number, Ca, discussed in the equations for dynamic contact angle is a balance of F_μ to F_c, which characterizes the magnitude of viscous flow to restoring surface tension forces. Considering the triple line, viscous and capillary forces are the main governing

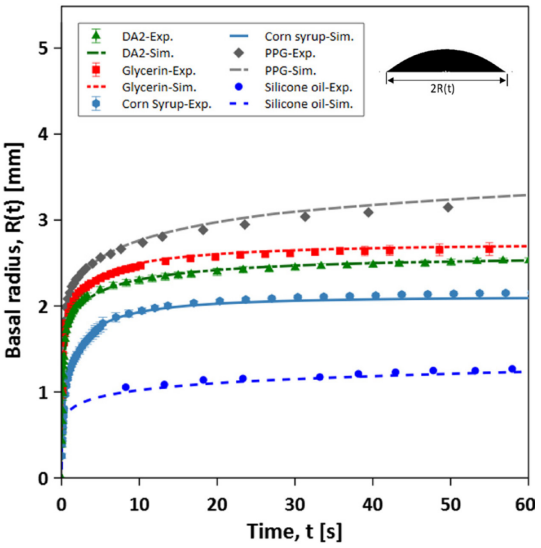

Figure 3: Validation of numerical model: comparison between simulation and experimental results of Glycerin, Corn syrup, DA2 resin, silicone oil [55] and PPG [32] for variation of basal radius over time.

Table 2: A summary of the driving forces governing droplet spreading [6]

Driving/Resistive forces	
Capillary Force	$F_c \sim \sigma R_0$
Gravitational Force	$F_g \sim \rho g R_0^3$
Viscous Force	$F_\mu \sim \mu R_0 \frac{dR}{dt}$
Inertial Force	$F_i \sim \rho R_0^2 \left(\frac{dR}{dt}\right)^2$

forces specially at the late stage of drop spreading. That is the reason Ca number can scale the dynamic contact angle data (see Fig. 2).

Our numerical simulations and models will only consider spreading dynamics in a regime where Bo $<$ 1 and Oh $>$ 1, such that gravitational effect matters, and the viscous resistance dominates the spreading process. As one of the primary applications of our interest is the bead-based additive manufacturing, it is conservative to argue that bead-based additive manufacturing is best operated in these bounds, i.e. Bo $<$ 1 and Oh $>$ 1. Note that operating bead-based printing outside of these bounds would result in a much more difficult to control bead/droplet dynamics, and therefore more difficult to optimize printing parameters. Therefore our numerical simulations and models will only consider spreading dynamics in these bounds.
Spreading is by definition a dynamic process and therefore it is useful to consider the different timescales that govern the spreading dynamics. If one were to observe a drop spreading on a substrate for Bo $<<$ 1 (no gravitational effect), one would initially observe a very fast spreading regime,a.k.a inertial regime, followed by a much slower viscous spreading regime [10, 6, 11, 12, 20]. These two regimes are said to be dominated by a capillary timescale, τ_c, and a viscous

timescale, τ_μ, respectively. For example, we can define a viscous timescale by supposing that viscous forces are on the order of capillary forces, i.e. $F_\mu \sim F_c$, which solving for τ_μ gives,

$$\tau_\mu = \frac{\mu R_0}{\sigma} \tag{8}$$

Furthermore, we can define a capillary timescale, τ_c by supposing that inertial forces are on the order of capillary forces, i.e. $F_i \sim F_c$, which solving for τ_c gives,

$$\tau_c = \sqrt{\frac{\rho R_0^3}{\sigma}} = \frac{\tau_\mu}{\mathrm{Oh}} \tag{9}$$

It has been shown that the characteristic time scale of duration of the inertial regime is $\tau \approx \mathrm{Oh}^{-0.25}\tau_c$ [6], which is in the order of milliseconds for small droplets with $Bo < 1$ and $Oh > 1$ bounds. It is safe to say that the inertial resistive forces against spreading can be ignored for droplet with those bounds compared to the whole time course of the spreading. Moreover, for the common bead-based processes with $Bo < 1$ and $\mathrm{Oh} > 1$, gravitational effects cannot be completely ignored. Therefore, the overall spreading timescale, τ_s, can be approximated by the balance of viscous resistive force and driving forces, i.e. $F_\mu \sim F_c + F_g$, given in Table 2 as follow:

$$\tau_s = \frac{\mu R_0}{\sigma + \rho g R_0^2} = \frac{\tau_\mu}{1 + \mathrm{Bo}} \tag{10}$$

The validated spreading numerical simulation will be used to evaluate the dynamic spreading of spherical droplets as a function of a range of experimental parameters. The above mentioned timescales, Eqs. 9-10, will be used to scale the physics of the spreading process and relate such dynamics to droplet spreading parameters. The goal is generalizing the results to develop master curves and spreading models that capture the shape of spherical drops in terms of basal radius and height as a function of time. These models and results are expected to be useful in predicting the spreading of deposited droplets for a wide range of processes, especially the bead-based additive manufacturing.

3.1. Spreading dynamics in complete wetting condition

This section focuses on the case of $\theta_s = 0$, known as complete wetting. Note that complete wetting means that the basal radius goes to infinity, or the finite size of the container. However, the spreading process is a weak power-law function and achieving equilibrium is computationally expensive. Therefore, practically speaking, the numerical simulations required a cutoff time. Similar to other works, we define a final spreading time where the spreading velocity of the contact line falls below 10^{-4} [mm/s], i.e. a 100 [nm/s] [60].

The first case that we simulate is that of a fixed Bo and Oh number. Figure 4a shows the measured basal radius as a function of time considering different fluid properties and varying initial drop radii such that Oh and Bo are equivalent for all cases, see inset. As discussed above, we clearly observe two different spreading regimes, i.e. fast inertial driven spreading followed by slow viscous driven spreading. Interestingly, the basal radius dynamics for all cases appear to have the same shape, but shifted vertically depending on initial droplet size and slightly horizontally due to fluid properties. This suggests that complete wetting spreading dynamics

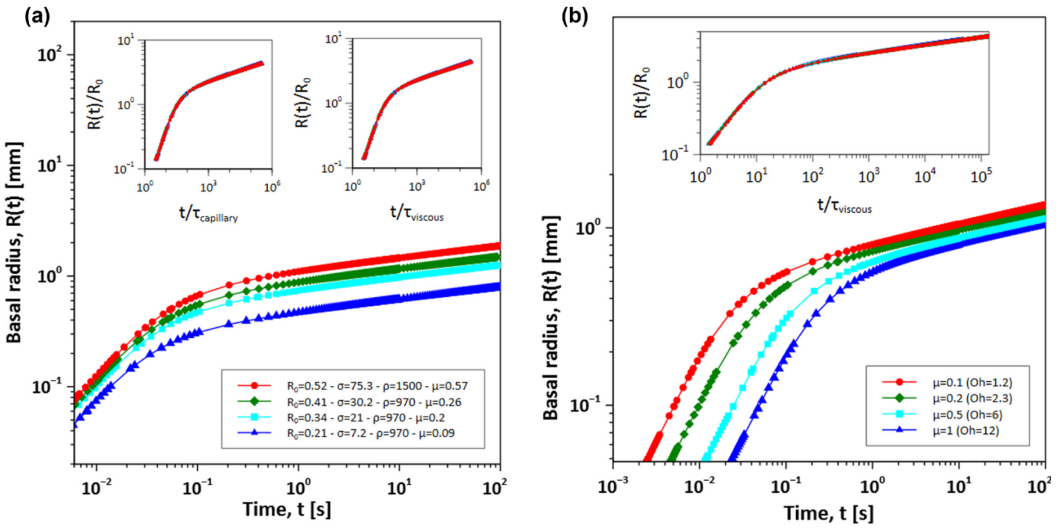

Figure 4: Time evolution of basal radius: **a)** for Oh $= 2.38$ and Bo $= 0.05$. Insets: scaled radius versus scaled time via the capillary timescale, $\tau_{\text{capillary}}$, and viscous timescale,τ_{viscous}, and **b)** for fluids with varying Oh and Bo $= 0.05$. Inset: scaled basal radius versus scaled time via viscous timescale. All fluid have the same properties as $\rho = 970\ kg/m^3$, $\sigma = 20.9\ mN/m$, and $R_0 = 0.34\ mm$ with different viscosity. Note that the insets show that all experimental conditions collapse onto a single master curve.

follow a law of similitude that depends on Bo and Oh.

The law of similitude is exemplified in the inset of Fig. 4a, whereby the normalized basal radius (a.k.a spreading coefficient) is plotted versus scaled time, scaled by τ_c in the left inset of Fig. 4a and τ_μ in the right inset of Fig. 4a. Both Figures show that all dynamics collapse onto a master curve regardless of the timescale, which generalizes the spreading solution to all parameters for a given Bo and Oh for $\theta = 0$. (Generalized spreading solution for a given Bo and Oh in terms of the change in the height of the droplet has been shown in Fig. S7) The reason for both timescales creating a master curve is due to the constant Oh for all simulations. According to Eq. 9, the capillary and viscous timescales are proportional when the Oh is constant. We hypothesized earlier that the correct timescale is τ_s. For constant Bo, τ_s, see Eq. 10, is proportional to the viscous timescale ($\tau_s \sim \tau_\mu$). Therefore, normalizing the time with τ_μ or τ_s collapses all the graphs onto a single master curve. These numerical results confirm previously reported literature results [1, 16, 10], which demonstrate a spreading master curve for a limited range of fluid properties.

The viscous timescale captures the spreading physics more completely than the capillary timescale. Although the τ_c collapsed the data above, this was due to the constant Oh. In the case of varying Oh, only τ_μ is capable of generating a master curve. Figure 4b shows the spreading dynamics of fluids with increasing values of Oh numbers (for Oh > 1), and constant Bo number. The counterpart of Fig.4b in terms of change in the height of the droplet has been shown in Fig. S8. As expected, fluids with higher Oh numbers exhibit slower increase in basal radius due to the larger energy dissipation at the contact line [10]. The inset in Fig.4b shows that scaling time with the viscous timescale (t/τ_μ) results in a master curve. As in the case of constant Bo

above, τ_s is proportional to τ_μ, and thus the data can be readily scaled with τ_s. Note that the τ_c does not collapse the data onto a master curve since τ_c is not proportional to τ_μ for varying Oh.

We showed that as long as the Bo is constant, the spreading dynamics of Newtonian fluids can be scaled using the viscous timescale (τ_μ), regardless of Oh. However, unlike Oh, changing Bo has a unique effect on the shape of basal radius spreading dynamics. For the fluids where the Bo is not the same, neither τ_s nor τ_μ can scale the spreading dynamics. In other words, for each Bo number, there is a mastercurve. Figure 5 shows the normalized basal radius and normalized droplet height as a function of the spreading time normalized by the viscous timescale for a range of Bo. Note that this figure is plotted log-linear and therefore looks different than the log-log plot of Fig. 4b. For higher Bo numbers, i.e. a stronger effect of gravity on the spreading dynamics, the basal radius spreads faster compared to lower Bo numbers. For $\mathrm{Bo} < 0.1$, the spreading evolution is very similar up to $R/R_0 = 4$, signifying that gravity has little effect on spreading below $\mathrm{Bo} = 0.1$. In other words, the dynamics for $\mathrm{Bo} = 0.01$, the red circles in Fig. 5, predicts the shape of all droplets for $\mathrm{Bo} \leq 0.1$. However, increasing the Bo number from 0.1 to 1 increases the basal radius spreading by more than 10% at later stages of spreading. One important takeaway message is that for $\theta_s = 0^\circ$, the zero Bond number assumption predicts droplet spreading very well for small normalized basal radius ($R(t)/R_0 < 3$), i.e. less than 5% error. In other words, the effect of gravity is not observed until sufficiently long normalized times. Using the master curves in Fig. 5, one can predict the spreading factor (R/R_0) at an arbitrary time, i.e., one can predict the shape of any drop at any time after deposition. For instance, a drop shape of R/R_0=2.5 for $\mathrm{Bo} = 0.01$, is achieved at t/τ_μ =600. Thus, by calculating τ_μ via the properties of the drop, i.e., density, viscosity and initial radius, the time to reach the specified shape is readily calculated. These results demonstrate that for perfect wetting the only dimensionless number that dictates the shape of changing basal radius with time is the Bo number. Figure 5 also contains the master curves corresponding to the change in the height of the droplet during spreading process. Like the basal radius, given the properties of droplet, i.e. Bo number and τ_μ, the height of the droplet can be predicted at a certain time. Using the values of both height and basal radius, the shape of the droplet can be fully characterized.

3.2. Spreading dynamics in partial wetting condition

When the static advancing contact angle is non-zero, a.k.a partial wetting, the spreading continues until Young's equation is satisfied. In other words, the dynamic contact angle decreases until the static advancing contact angle is achieved. Therefore, there are two parameters that dictate basal radius spreading dynamics: Bo number and θ_s. Numerical simulations with varying both Bo and θ_s were performed and analyzed using the same scaling analysis as the perfect wetting condition discussed above. Figure 6a shows a series of scaled basal radius master curves for different Bo numbers and different θ_s. Figure 6b shows master curves for the scaled height of the droplets. Figure 6a shows that increasing Bo acts to increase the rate of spreading for all values of θ_s, although the effect is more noticeable at smaller θ_s, i.e. higher Bo increases basal radius by $\approx$5% and > 10% for $\theta_s = 45$ and 10, respectively, at long normalized times, $t/\tau_{viscous} > 10^4$. Thus, the zero Bond number assumption is relatively good for all basal radii for large θ_s. The effect of increasing θ_s is to reduce the effect of Bo and achieve a constant basal radius. As expected, for a given Bo all spreading curves are identical at short time, i.e. $t/\tau_{viscous}$<20, regardless of θ_s.

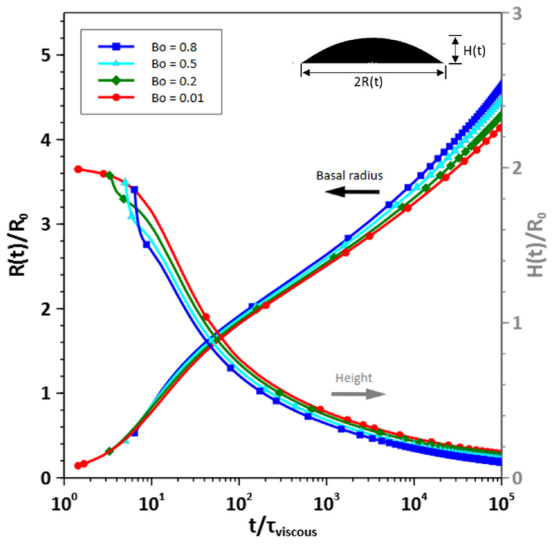

Figure 5: Complete wetting Newtonian droplet master curve: scaled basal radius and scaled height versus scaled time via viscous timescale for fluids with different Bo numbers.

Figure 6 is quite useful in predicting the spreading of droplets in a wide range of applications, where inertial impact on the surface can be ignored. For example, given the value of Bo number and θ_s, which are intrinsic properties of the system, the shape of the drop can be predicted at any given time via the value of $\tau_{viscous}$. This information is particularly useful in bead-based additive manufacturing as printing parameters, such as layer width and height can be adjusted to accommodate the true shape of the bead. This will certainly improve the dimensional accuracy of printed parts in droplet/bead-based additive manufacturing processes, and reduce the need for wasteful edisonian approaches to print quality.

3.2.1. Final shape prediction

There have been a few theoretical attempts to develop a theory for the equilibrium shape of a droplet deposited on a substrate [61, 62]. The numerical data and scaling arguments presented here provide a platform, in which to test these theories and possibly generalize the spreading theories. For example, de Gennes et al. [61] developed a theoretical relation for the final height of heavy droplets, i.e. Bo > 1 after deposition. Using the balance between hydrostatic pressure inside a pancake-like droplet with the surface forces, the final height can be estimated as $H_f = 2l\sin(\theta_s/2)$, where l is the capillary length of droplet. However, this relation is limited to the droplets with high Bo numbers (Bo > 1, pancake-like shape). Yonemoto and Kunugi [62] modified de Gennes's theory using the work-energy balance and incorporated work-energy in the vertical direction at the contact line during the change in the droplet height. Yonemoto and Kunugi [62] derived a theoretical relation between the final height and final basal radius of a droplet at a given volume. Yonemoto and Kunugi's theory can be rearranged in terms of Bo number and θ_s, for comparison to this work, and is given by:

$$\frac{2\mathrm{Bo}}{3}\frac{H_f}{R} = \left(\frac{R_f}{R}\right)^2 (1-\cos\theta_s)\left(\frac{R_f}{R}-\frac{H_f}{R}\right)\sin\theta_s \qquad (11)$$

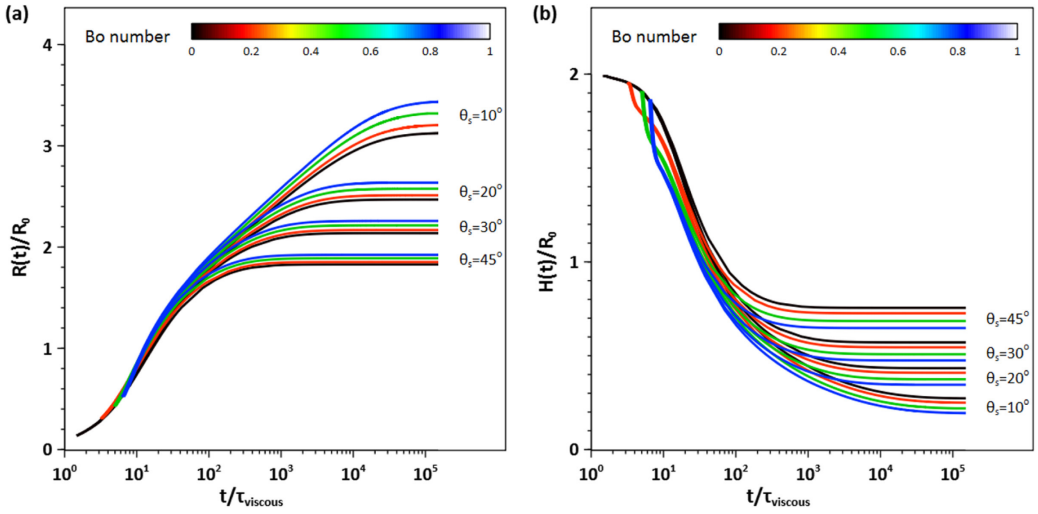

Figure 6: Partial wetting Newtonian droplet master curves: **a)** scaled basal radius and **b)** scaled height of the droplet versus scaled time via viscous timescale for fluids with different Bo numbers and Θ_s.

where R_f and H_f are the final spreading radius and height, respectively. One interesting observation is that the theory only depends on the value of Bo and Θ_s, which is in line with our master curves in Fig. 6. Note that this equation is not particularly useful, since there are two unknowns, height and radius, and therefore no unique solution. However, this equation should be able to solve for H_f given R_f, and vice-versa. Therefore, development of a correlation to independently predict the final basal radius of the droplet and coupling with Eq. 11 seems quite useful in characterization of the final shape of the droplet. The numerical simulations are useful in developing a correlation between scaled basal radius, Bo and Θ_s. We calculated the final shape of a droplet for Bo numbers between 0.01 and 1, and Θ_s between 0° and 90°. Figure 7 illustrates the variation of scaled final basal radius (R_f/R_0) with both Bo number and Θ_s. As discussed in the dynamic data, increasing the Bo number increases the steady state value of R_f/R_0; while increasing Θ_s, arrests the droplet shape at lower R_f/R_0 values. Moreover, by increasing Θ_s, the dependency of R_f/R_0 on the Bo number decreases.

We observe from Fig. 7 that R_f/R_0 varies with Θ_s as a power-law, whose power depends on the value of Bo. We propose the following empirical model:

$$\frac{R_f}{R_0} = \alpha \left(\frac{\Theta_s}{\beta - \gamma \Theta_s} \right)^{\delta} \tag{12}$$

where α, β, γ, and δ are model parameters to be fitted to the data. Note that γ and δ are expected to be functions of Bo. Furthermore, the model must capture two important limits; first, at complete wetting condition ($\Theta_s = 0$), $R_f/R_0 \to \infty$. Second, at $\Theta_s = 90°$ and at very low Bo numbers (where the droplet resembles spherical cap), $R_f/R_0 \to \sqrt{2}$. Using the Generalized Reduced Gradient (GRG) nonlinear fitting algorithm [63], the best-fit model parameters are given in Table 3. The coefficient of determination, typically denoted R^2, is used to quantify the variation

of the best-fit model to the data. In our case, $R^2 = 0.99$, which shows excellent agreement

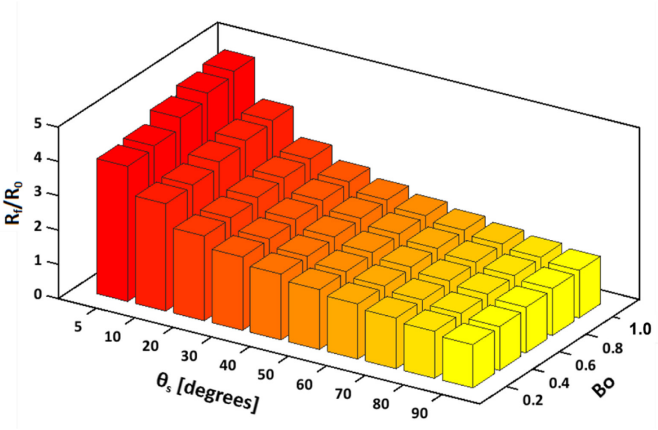

Figure 7: Final shape of deposited droplet in terms of scaled final basal radius (R_f/R_0) vs Bo number and Θ_s.

Table 3: Best fit model parameters for Eq. 12 determined using the Generalized Reduced Gradient nonlinear fitting algorithm.

Parameter	Best-fit value
α	2.42
β	0.44
γ(Bo)	0.31+0.10Bo
δ(Bo)	0.17Bo-0.15

between the predicted value and experimental data. We compared the best-fit parameters for Eq. 12 and the numerically determined scaled final basal radii as a function of static advancing contact angle for Bo $= 0.01$ and Bo $= 1$. The model and simulated data are in excellent agreement for the two extreme values of Bo, see Supplementary Information, Fig. S9.

To further validate our empirical model, we compared the model with previously reported experimental data for pure ethanol and a binary mixture of ethanol and water[62]. Table 4 shows the experimentally measured values of fluid properties, volume and final basal radius [62]. We plotted the experimental data based on final basal radius vs Bo number for each case and compared it with the prediction of Eq.12. As seen in Fig. 8, the predicted final basal radii by the empirical model with the best-fit parameters in Table 3 are in excellent agreement with experimental data of [62].

Coupling our developed correlation (Eq. 12) with the Eq. 11, the final height of the droplets can be predicted at different Bo and Θ_s. Figure 9 shows the scaled droplet height (H_f/R_0) as a function of R_f/R_0 for two values of Bo and varying Θ_s. The lines reflect the estimation from Eqs. 11 and 12. As it can be seen, the empirical model prediction for height of the droplet is in excellent agreement with the numerical simulation results for Bo $= 0.01$, and is in good agreement for Bo $= 1$. For the latter, the equations slightly under predict the droplet height. Overall, it can be concluded that the empirical correlation of Eq. 12 coupled with Eq. 11 give predictions of both final basal radius and final height for a range of Bo and Θ_s within 10% or better.

Table 4: Experimental data of fluid properties, volume, and final shape in terms of basal radius for pure ethanol and binary mixtures of water/ethanol reported in [62]

Fluid	σ (J/m^2)	ρ (kg/m^3)	θ_s (deg.)	V (μL)	Bo	R_f (mm)	Model R_f (mm)
Pure Ethanol	0.0211	789.2	35	5	0.41	2.251	2.178
				10	0.65	2.723	2.779
				20	1.03	3.637	3.582
Water/Ethanol	0.0312	911.4	76	5	0.32	1.539	1.564
				10	0.51	1.944	2.009
				20	0.81	2.521	2.605

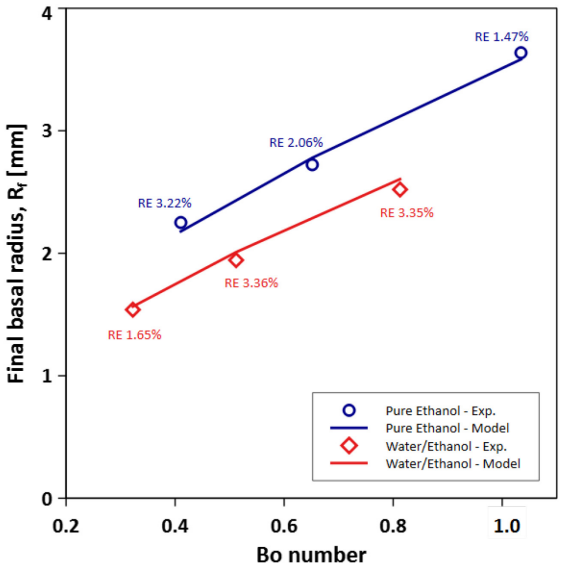

Figure 8: Comparison of empirical model prediction with the experimental data of pure ethanol and water/ethanol binary mixture reported in [62]. Numbers indicate the relative error.

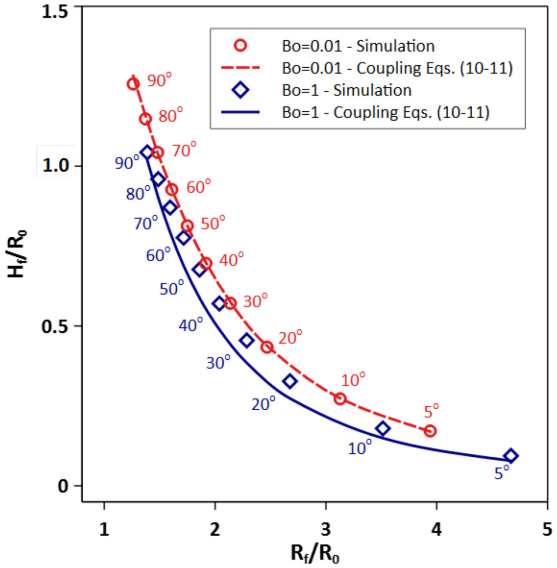

Figure 9: Scaled steady state height of the droplet versus scaled steady state basal radius at different Bo numbers and θ_s. Comparison of Eqs. 11 and 12) (lines) with numerical simulation results (symbols).

4. Conclusion

This work presents a generalized scaling theory for the problem of spontaneous dynamic spreading of Newtonian fluids on a flat substrate using advanced numerical tools. While the problem has been discussed in the literature over many decades [42, 6, 64, 65], this work presents the first generalized description of droplet spreading and scaling approach taking into account the influence of gravity and both complete and partial wetting conditions. We developed and validated our model using experimental data and a generalized dynamic contact angle model for the triple point contact line boundary condition. One important aspect of this work is the use of a dynamic contact angle model as a boundary condition that has been experimentally demonstrated to be independent of fluid parameters.

The experimentally validated numerical model was used to predict the dynamic spreading of complete wetting and partial wetting conditions for a range of Bo numbers. We demonstrated that the Bo, $\tau_{viscous}$, θ_s are the three important parameters that control the spreading. For a specific Bo and θ_s, The spreading dynamic curves, i.e. evolution of basal radius, collapse onto a single master curve by scaling the spreading time with $\tau_{viscous}$. The only limitation of the model is that it considers no impact of the droplet on the substrate, and therefore the dynamic spreading phenomena is only applicable to specific spreading scenarios.

For partial wetting systems, the model is used to predict final droplet shape as a function of Bo and θ_s. An empirical model is presented that captures the scaled radius as a function of both parameters. The best-fit parameters are coupled with a theoretical model to predict drop height. The coupled equations are validated using numerical and experimental data. These equations offer a simple predictive tool to steady state spreading shape as a function of Bo and θ_s within 10% error. This study presents the first predictive model for both dynamic and equilibrium shape of a droplet on a solid substrate taking into account the static advancing contact angle. As a

practical application, these predictive models (dynamic master curves and the empirical model) can be incorporated into the bead-based additive manufacturing [1, 56, 66] through printing parameterization software to take spreading into account and accurately determine the optimum droplet diameter, spacing, and final layer height. The position of adjacent droplets and the retraction height of the nozzle can be automatically adjusted based on the spreading of printed beads. Moreover, such empirical models for prediction of the final shape of a droplet are in high demand in other industries such as droplet fabrication of optical micro lenses [4, 67]. The author's are working to extend this model to non-Newtonian spreading droplets and cylindrical filaments for application to DIW and filament extrusion additive manufacturing methods.

5. Author's Contributions

A. Azimi Yancheshme: Conceptualization, Methodology, Software, Validation, Visualization, Writing/Original Draft Preparation. **G. R. Palmese**: Conceptualization, Funding Acquisition, Writing/Review & Editing. **N. J. Alvarez**: Conceptualization, Funding Acquisition, Methodology, Supervision, Writing/Review & Editing.

6. Supplementary Information

See Supplementary Material for additional figures that validate the numerical model.

7. Acknowledgements

Research was sponsored by the Army Research Laboratory and was accomplished under Cooperative Agreement Number W911NF-17-2- 0227. The views and conclusions contained in this document are those of the authors and should not be interpreted as representing the official policies, either expressed or implied, of the Army Research Laboratory or the U.S. Government. The U.S. Government is authorized to reproduce and distribute reprints for Government purposes not withstanding any copyright notation herein. NJA was also supported by the National Science Foundation under grant no. CBET-1847140.

8. Author Declaration

The authors declare that they have no known competing financial interests or personal relationships that could have appeared to influence the work reported in this paper.

References

[1] V. S. Sivasankar, H. S. Sachar, S. Sinha, D. R. Hines, S. Das, 3d printed microdroplet curing: Unravelling the physics of on-spot photopolymerization, ACS Applied Polymer Materials 2 (2) (2020) 966–976.
[2] R. De Ruiter, L. Royon, J. H. Snoeijer, P. Brunet, Drop spreading and gelation of thermoresponsive polymers, Soft Matter 14 (16) (2018) 3096–3104.
[3] J. E. Sprittles, Dynamic wetting/dewetting processes in complex liquid-solid systems, Ph.D. thesis, University of Birmingham (2010).
[4] Y.-L. Sung, J. Jeang, C.-H. Lee, W.-C. Shih, Fabricating optical lenses by inkjet printing and heat-assisted in situ curing of polydimethylsiloxane for smartphone microscopy, Journal of biomedical optics 20 (4) (2015) 047005.
[5] W. Bou-Zeid, D. Brutin, Beyond tanner's law: Role of contact line evaporation on the spreading of viscous droplet, Interfacial Phenomena and Heat Transfer 3 (3) (2015).

[6] A.-L. Biance, C. Clanet, D. Quéré, First steps in the spreading of a liquid droplet, Physical Review E 69 (1) (2004) 016301.
[7] T. Young, Iii. an essay on the cohesion of fluids, Philosophical transactions of the royal society of London (95) (1805) 65–87.
[8] V. Starov, V. Kalinin, J.-D. Chen, Spreading of liquid drops over dry surfaces, Advances in colloid and interface science 50 (1994) 187–221.
[9] P.-G. De Gennes, F. Brochard-Wyart, D. Quéré, et al., Capillarity and wetting phenomena: drops, bubbles, pearls, waves, Vol. 315, Springer, 2004.
[10] A. Eddi, K. G. Winkels, J. H. Snoeijer, Short time dynamics of viscous drop spreading, Physics of fluids 25 (1) (2013) 013102.
[11] K. G. Winkels, J. H. Weijs, A. Eddi, J. H. Snoeijer, Initial spreading of low-viscosity drops on partially wetting surfaces, Physical Review E 85 (5) (2012) 055301.
[12] D. Bonn, J. Eggers, J. Indekeu, J. Meunier, E. Rolley, Wetting and spreading, Reviews of modern physics 81 (2) (2009) 739.
[13] O. Voinov, Gravity-induced spreading of a drop of a viscous fluid over a surface, Journal of applied mechanics and technical physics 40 (3) (1999) 412–419.
[14] A. Cazabat, M. C. Stuart, Dynamics of wetting: effects of surface roughness, The Journal of Physical Chemistry 90 (22) (1986) 5845–5849.
[15] A. Carlson, G. Bellani, G. Amberg, Universality in dynamic wetting dominated by contact-line friction, Physical Review E 85 (4) (2012) 045302.
[16] J. C. Bird, S. Mandre, H. A. Stone, Short-time dynamics of partial wetting, Physical review letters 100 (23) (2008) 234501.
[17] M. J. De Ruijter, J. De Coninck, G. Oshanin, Droplet spreading: partial wetting regime revisited, Langmuir 15 (6) (1999) 2209–2216.
[18] L. Chen, E. Bonaccurso, Effects of surface wettability and liquid viscosity on the dynamic wetting of individual drops, Physical Review E 90 (2) (2014) 022401.
[19] L. Courbin, J. C. Bird, M. Reyssat, H. Stone, Dynamics of wetting: from inertial spreading to viscous imbibition, Journal of Physics: Condensed Matter 21 (46) (2009) 464127.
[20] H. Grewal, H. Nam Kim, I.-J. Cho, E.-S. Yoon, Role of viscous dissipative processes on the wetting of textured surfaces, Scientific reports 5 (1) (2015) 1–11.
[21] L. Shi, Y. Liu, H. Lu, Y. Meng, G. Hu, Y. Tian, Viscous force retards initial droplet spreading, The Journal of Physical Chemistry C 121 (40) (2017) 22054–22059.
[22] S. Rafaï, D. Sarker, V. Bergeron, J. Meunier, D. Bonn, Superspreading: aqueous surfactant drops spreading on hydrophobic surfaces, Langmuir 18 (26) (2002) 10486–10488.
[23] L. Tanner, The spreading of silicone oil drops on horizontal surfaces, Journal of Physics D: Applied Physics 12 (9) (1979) 1473.
[24] J. Lopez, C. A. Miller, E. Ruckenstein, Spreading kinetics of liquid drops on solids, Journal of Colloid and Interface Science 56 (3) (1976) 460–468.
[25] P. Levinson, A. Cazabat, M. C. Stuart, F. Heslot, S. Nicolet, The spreading of macroscopic droplets, Revue de physique appliquee 23 (6) (1988) 1009–1016.
[26] A. Milchev, A. Milchev, K. Binder, Nanodroplets on a solid plane: wetting and spreading in a monte carlo simulation, Computer physics communications 146 (1) (2002) 38–53.
[27] G. He, N. Hadjiconstantinou, A molecular view of tanner's law: molecular dynamics simulations of droplet spreading, Journal of Fluid Mechanics 497 (2003) 123–132.
[28] A. Milchev, K. Binder, Droplet spreading: A monte carlo test of tanner's law, The Journal of chemical physics 116 (17) (2002) 7691–7694.
[29] S. P. Thampi, I. Pagonabarraga, R. Adhikari, R. Govindarajan, Universal evolution of a viscous–capillary spreading drop, Soft matter 12 (28) (2016) 6073–6078.
[30] H. Ding, P. D. Spelt, Inertial effects in droplet spreading: a comparison between diffuse-interface and level-set simulations, Journal of fluid mechanics 576 (2007) 287–296.
[31] S. Kalliadasis, H.-C. Chang, Dynamics of liquid spreading on solid surfaces, Industrial & engineering chemistry research 35 (9) (1996) 2860–2874.
[32] X. Wang, Y. Zhang, D. Lee, X. Peng, Spreading of completely wetting or partially wetting power-law fluid on solid surface, Langmuir 23 (18) (2007) 9258–9262.
[33] D. Erickson, B. Blackmore, D. Li, An energy balance approach to modeling the hydrodynamically driven spreading of a liquid drop, Colloids and Surfaces A: Physicochemical and Engineering Aspects 182 (1-3) (2001) 109–122.
[34] J. Madejski, Solidification in flow through channels and into cavities, International Journal of Heat and Mass Transfer 19 (12) (1976) 1351–1356.
[35] Y. Gu, D. Li, A model for a liquid drop spreading on a solid surface, Colloids and Surfaces A: Physicochemical

and Engineering Aspects 142 (2-3) (1998) 243–256.
[36] Y. Gu, D. Li, Liquid drop spreading on solid surfaces at low impact speeds, Colloids and Surfaces A: Physicochemical and Engineering Aspects 163 (2-3) (2000) 239–245.
[37] O. Voinov, Hydrodynamics of wetting, Fluid dynamics 11 (5) (1976) 714–721.
[38] R. Cox, The dynamics of the spreading of liquids on a solid surface. part 1. viscous flow, Journal of fluid mechanics 168 (1986) 169–194.
[39] T. Blake, J. Haynes, Kinetics of liquidliquid displacement, Journal of colloid and interface science 30 (3) (1969) 421–423.
[40] P. Petrov, I. Petrov, A combined molecular-hydrodynamic approach to wetting kinetics, Langmuir 8 (7) (1992) 1762–1767.
[41] M. Härth, D. W. Schubert, Simple approach for spreading dynamics of polymeric fluids, Macromolecular Chemistry and Physics 213 (6) (2012) 654–665.
[42] S. Reznik, A. Yarin, Spreading of an axisymmetric viscous drop due to gravity and capillarity on a dry horizontal wall, International journal of multiphase flow 28 (9) (2002) 1437–1457.
[43] N. T. Chamakos, M. E. Kavousanakis, A. G. Boudouvis, A. G. Papathanasiou, Droplet spreading on rough surfaces: Tackling the contact line boundary condition, Physics of Fluids 28 (2) (2016) 022105.
[44] C. Neto, D. R. Evans, E. Bonaccurso, H.-J. Butt, V. S. Craig, Boundary slip in newtonian liquids: a review of experimental studies, Reports on progress in physics 68 (12) (2005) 2859.
[45] T. Lee, E. Charrault, C. Neto, Interfacial slip on rough, patterned and soft surfaces: A review of experiments and simulations, Advances in colloid and interface science 210 (2014) 21–38.
[46] Y. D. Shikhmurzaev, Singularities at the moving contact line. mathematical, physical and computational aspects, Physica D: Nonlinear Phenomena 217 (2) (2006) 121–133.
[47] V. Dussan, The moving contact line: the slip boundary condition, Journal of Fluid Mechanics 77 (4) (1976) 665–684.
[48] E. Dussan, On the spreading of liquids on solid surfaces: static and dynamic contact lines, Annual Review of Fluid Mechanics 11 (1) (1979) 371–400.
[49] R. L. Hoffman, A study of the advancing interface. i. interface shape in liquid—gas systems, Journal of colloid and interface science 50 (2) (1975) 228–241.
[50] T.-S. Jiang, O. Soo-Gun, J. C. Slattery, Correlation for dynamic contact angle, Journal of colloid and interface science 69 (1) (1979) 74–77.
[51] M. Bracke, F. D. Voeght, P. Joos, The kinetics of wetting: the dynamic contact angle, Trends in Colloid and Interface Science III (1989) 142–149.
[52] S. Kistler, Wettability, edited by jc berg marcel dekker, New York (1993).
[53] Š. Šikalo, H.-D. Wilhelm, I. Roisman, S. Jakirlic´, C. Tropea, Dynamic contact angle of spreading droplets: Experiments and simulations, Physics of Fluids 17 (6) (2005) 062103.
[54] J. Tu, K. Makarian, N. J. Alvarez, G. R. Palmese, Formulation of a model resin system for benchmarking processing-property relationships in high-performance photo 3d printing applications, Materials 13 (18) (2020) 4109.
[55] J.-D. Chen, Experiments on a spreading drop and its contact angle on a solid, Journal of colloid and interface science 122 (1) (1988) 60–72.
[56] J. Xie, R. Randolph, G. Simmons, M. Vinciguerra, S. Suri, N. Bonini, A. Root, P. V. Hull, A. D. Mazzeo, Spreading of fast-curing, thermosetting silicones, Applied Physics Letters 115 (25) (2019) 253701.
[57] B. S. Yilbas, A. Al-Sharafi, H. Ali, N. Al-Aqeeli, Dynamics of a water droplet on a hydrophobic inclined surface: influence of droplet size and surface inclination angle on droplet rolling, Rsc Advances 7 (77) (2017) 48806–48818.
[58] N. J. Alvarez, L. M. Walker, S. L. Anna, A non-gradient based algorithm for the determination of surface tension from a pendant drop: Application to low bond number drop shapes, Journal of colloid and interface science 333 (2) (2009) 557–562.
[59] B. Derby, Inkjet printing of functional and structural materials: fluid property requirements, feature stability, and resolution, Annual Review of Materials Research 40 (2010) 395–414.
[60] X. Yu, R. Hu, L. Zhou, H. Wu, X. Luo, Spreading and curing behaviors of a thermosetting droplet- silicone on a heated surface, Journal of Harbin Institute of Technology (New Series) 26 (4) (2019) 1–8.
[61] P.-G. De Gennes, Wetting: statics and dynamics, Reviews of modern physics 57 (3) (1985) 827.
[62] Y. Yonemoto, T. Kunugi, Theoretical model of droplet wettability on a low-surface-energy solid under the influence of gravity, The Scientific World Journal 2014 (2014).
[63] L. S. Lasdon, R. L. Fox, M. W. Ratner, Nonlinear optimization using the generalized reduced gradient method, Revue française d'automatique, informatique, recherche opérationnelle. Recherche opérationnelle 8 (V3) (1974) 73–103.
[64] A. M. Alteraifi, D. Sherif, A. Moet, Interfacial effects in the spreading kinetics of liquid droplets on solid substrates, Journal of colloid and interface science 264 (1) (2003) 221–227.

[65] F. Brochard-Wyart, H. Hervet, C. Redon, F. Rondelez, Spreading of "heavy" droplets: I. theory, Journal of colloid and interface science 142 (2) (1991) 518–527.
[66] B. Mueller, Additive manufacturing technologies–rapid prototyping to direct digital manufacturing, Assembly Automation (2012).
[67] Y.-L. Sung, J. Garan, Z. Hu, X. Shan, W.-C. Shih, Modeling the surface of fast-cured polymer droplet lenses for precision fabrication, Applied optics 57 (35) (2018) 10342–10347.